Synthesis and characterizations of pure size-controlled palladium oxide (PdO) nanoparticles via a modified thermal treatment route

Ayser S. Keiteb[1] and Mohammed M. Sabri[2]

[1]College of Health and Medical Technologies, Middle Technical University, Baghdad, Iraq

[2]Department of Physics, Faculty of Science and Health, Koya University, Koya 44023, Kurdistan Region – F.R. Iraq

Abstract

Using deionized water, polyvinylpyrrolidone as a capping agent, palladium (II) nitrate dihydrate, Pd (NO3)2.2H2O as the metal precursor and a modified thermal treatment technique, palladium oxide (PdO) with nanocrystalline structures was successfully produced. The unadulterated nanocrystalline was obtained by calcining the homogenous solution directly to produce the powder. Energy dispersive x-ray (EDX), Fourier-transform infrared spectroscopy (FTIR) and x-ray diffraction (XRD) were used to confirm this. PVP functions to cap the agglomeration, stabilize particle growth and disintegrate at 436 °C when heated. As crystallinity rose, different peak spectra in FTIR spectra were associated with higher temperatures. PVP was used to boost the calcination temperatures from 500 to 800 °C in order to modify the size and optical properties of the nanoparticles. The average particle sizes from XRD spectra and transmission electron microscopy (TEM) micrographs were found to be 22 nm at 500 °C and 46 nm at 800 °C as the calcination temperature increased, according to Scherrer's equation, which is in good agreement with TEM particle size estimations. Utilizing ultraviolet-visible (UV-Vis) spectrophotometer, the optical properties were investigated and discovered that the fused boundaries and quick enlargement of the particle surface area caused the band gap energy to fall with increasing calcination temperature, from 2.09 eV at 500 °C to 1.63 eV at 800 °C. Size-controlled PdO NPs were easily produced with a decrease in synthesis time and energy usage by excluding drying procedure (24 hours) from the current heat treatment method. These nanoparticles are appropriate for mass production of various applications.

1 Introduction

Nanotechnology has been reported as a breakthrough in the twenty first century of science and engineering in the synthesizing of smaller-sized materials having substantial chemical, physical and electronic properties at atomic scale [1]. A lot of interest has been gained for metal/metal oxide nanostructures and continues, attributed to their morphology and dimensions, electrical, mechanical as well as photosensitive characteristics, together with their exceptional resistance to rust and oxidation. In comparison to their bulk counterpart, it has been reported that nanoparticles

(NPs) exhibit significant efficiency as a result to their higher surface-to-volume ratio [2]. Extensive studies related to various metal nanoparticles have been published, while the research on their oxide counterpart is somewhat limited. In the past, palladium as a member of the platinum group metals (PGMs) and group ten in the periodic table was mainly known as a noble metal. Palladium is a chemical element of an atomic number of 46 and it is a silvery-white lustrous rare metal [3]. Its distinct catalytic activity was most likely only brought to light by the quick hydrogen absorption into bulk palladium.

At the beginning of the twenty-first century, detailed studies of the electron structure of palladium atom/nanocluster/nanoparticles launched a new understanding of the selective catalytic activity of this noble metal [4]. Out of all the platinum group metals (PGMs), which consist of platinum (Pt), rhodium (Rh), ruthenium (Ru), iridium (Ir) and osmium (Os), palladium has the lowest melting point and the least dense [5]. In addition, a unique phenomenon belonging to palladium is that the fifth O-shell in palladium's electron configuration is empty and this influences on its properties and take it out of that of ten group elements [6]. Recently, Pd and PdO NPs have received significant attention among other noble metal NPs due to their excellent chemical stability, thermal stability, catalytic activity, low cost as well as easy recovery [7-9]. Nano-scaled Pd NPs are of a significant importance due to their applications such as catalytic materials [10-14], oxidation, hydrogenation, low temperature C-C bond formation [15], electrochemical reactions in fuel cells [16-17], hydrogen storage [18], cross-coupling reaction [19], and gas sensing [20-22]. Pd NPs are unstable under annealing temperature, Palladium nanoparticles can oxidize to a number of different oxidation states from 0 to +4 [23-26]. In addition to the common unique characterizations of metals, the noble palladium nanoparticles (Pd NPs) have excellent physicochemical properties such as high thermal stability, good chemical stability, remarkable photocatalytic activity, electronic properties, optical properties and low cost [27-28].

The most significant oxidation state is monoxide (PdO), dioxide (PdO_2), trioxide (PdO_3) and hydrated sesquioxide ($Pd_2O_3.xH_2O$) [29]. In particular, palladium oxide (PdO) is attractive transition metal oxide due to their unusual physical and chemical properties as well as a wide range of technological applications such as in catalysis of methane combustion [30-31], CO oxidation [32-33], methanol oxidation [34], sensors [35] and photo-electrolysis [36]. Palladium oxide nanoparticles are an emerging focus in nanotechnology and materials science, characterized by their small size covering a few to tens of nanometers. These nanoparticles exhibit unique physical and chemical properties due to their high surface area-to-volume ratio and quantum confinement effects [37-38]. The synthesis and characterization of these nanoparticles have garnered significant interest, driven by their diverse applications across various fields. In addition, since palladium can be oxidized into palladium oxide (PdO), it is useful to pay significant consideration to the preparation of the pure and the alloyed palladium films, heterostructures as well as nanoparticles prepared on different substrates [39].

Palladium oxide nanoparticles have demonstrated significant potential in catalysis [40-41], leveraging their high surface area and electronic properties to enhance catalytic efficiency [42]. They are utilized as catalysts in crucial reactions such as the Suzuki-Miyaura cross-coupling reaction, highlighting their importance in organic synthesis [43]. Additionally, these nanoparticles, when supported on nitrogen-doped carbon, have proven effective as electrocatalysts for ethanol

oxidation reactions, showcasing their promise in energy conversion technologies [44]. In sensing applications, palladium oxide nanoparticles exhibit sensitivity to gases such as hydrogen and carbon monoxide, making them valuable in gas sensing devices. Their potential in biomedical applications, including drug delivery systems and bioimaging, is also being explored. Moreover, these nanostructures have shown efficacy in advanced oxidation processes used for wastewater treatment, underscoring their robust catalytic properties and environmental applications [45], as well as electrochemical applications [46]. It is important to say that a variety of approaches have been utilized to synthesis palladium oxide (PdO) nanoparticles. These include green synthesis technique [47-49], sputtering [50], ion or electron beam deposition [51], laser ablation [52-53], sol-gel [54], aqueous method [55], solution combustion method [56], microwave-assisted thermo-hydrolyzation [57], microwave irradiation method [58], combination of hydrothermal and calcination approaches [59], and controlled thermal decomposition method [3].

A countless research papers have been published regarding the synthesis of palladium nanoparticles, whereas only few ones reported the synthesis of palladium oxide (PdO) nanoparticles [60-61]. This research paper aimed at synthesizing palladium oxide (PdO) nanoparticles via a modified thermal treatment route followed by a suitable characterization. By eliminating the drying process from the current thermal treatment method, the size-controlled PdO NPs were produced in an accessible manner with a lower synthesis time and energy consumption, and the resulting PdO nanoparticles are suitable for mass production of a variety of applications.

2 Materials and Methods

2.1 Materials and resources

Sigma Aldrich provided the polyvinylpyrrolidone (PVP MW = 58000 g/mol) stock that was utilized as a capping agent. Deionized water was utilized as a solvent and palladium (II) nitrate dehydrates Pd (NO3)2.2H2O as a metal precursor. Sigma-Aldrich Chemistry provided the high purity stock (MW = 285.36 g/mol). Every chemical was utilized without any additional purification. 3 g of PVP powder is dissolved in 100 mL of deionized water at 70 °C, and the mixture is magnetically agitated for two hours to create the PVP solution. A semitransparent solution with no discernible material precipitation was achieved by adding 0.2 mmol of the metal precursor to the PVP solution and stirring constantly for a further two hours. The mixture directly placed in an alumina crucible for calcination at different temperatures ranging from 500 to 800 °C in a retention time of 3 h [62-63], to decompose the polymer and to crystallize the metal oxide nanoparticles.

2.2 Methods of characterization

Thermal analysis of the original solution dried at 30 °C was investigated using thermogravimetric analysis (TGA) and derivative thermogravimetry analysis (DTG) in the presence of N_2 with a heating rate of 10 °C/min above room temperature to 1000 °C in order to enhance the heat treatment program. This was done using a Perkin Elmer Thermal Analyzer model TGA7/DTA7. The Perkin Elmer Spectrum 1650 was utilized to analyze the chemical makeup of the materials

using Fourier transform infrared spectroscopy (FTIR). Energy dispersive x-ray (EDX) measurements were conducted using a variable pressure scanning electron microscope (VPSEM, LEO 1455) in conjunction with an Oxford INCA EDX 300 microanalysis attachment. The x-ray diffraction (XRD) method was used to determine the crystal phase of the produced samples using a Shimadzu-6000 diffractometer and CuKα (0.154 nm) radiation. The morphology and average particle size of the nanocrystalline powder were evaluated using the field emission scanning electron microscopy (FESEM) of type Joel JSM-7500f and the Hitachi H-7100 transmission electron microscope (TEM) operating at an accelerating voltage of 100 kV. The average size and size distribution of the nanoparticles were determined using image tool software. The samples' optical reflectance spectra were recorded using the Shimadzu-UV1650PC SHIMADZU UV-Vis spectrometer. The band gap energy was then determined from the reflectance spectra using the Kubelka-Munk function. All of the previously described measuring tools were calibrated to ensure accuracy and precision prior to conducting the tests, if required.

3 Results and Discussion

3.1 The role of PVP in synthesis process

Conferring to previous studies [64-66], the use of PVP in nanoparticles synthesis is very imperative as it plays four crucial roles: control the growth of nanoparticles, limit the agglomeration of nanoparticles, enhance the degree of particles crystallinity, and produce uniform particle size distribution. By sterically and electrostatically stabilizing the amide groups of the pyrrolidone rings and the methylene groups, PVP functions as a stabilizer or a mediator for the dissolution of complicated metallic salts in the first phase of creating the first solution. Palladium (II) nitrate dehydrates are dissolved in PVP solution, forming strong ionic interactions between the polymeric chain's amide group and the metallic ions Pd2+. Nanoparticles with a homogeneous distribution are often formed when metallic ions are uniformly immobilized in the voids of polymer chains. In the calcination step, although the organic matters will be decomposed to gasses such as N_2, NO, CO, or CO_2, trace of carbon residual that bonded on the surface of nanoparticles, which takes higher temperatures to decompose as shown by the weight loss in Fig. 1, can protect them from uncontrolled growth and agglomeration [65-67].

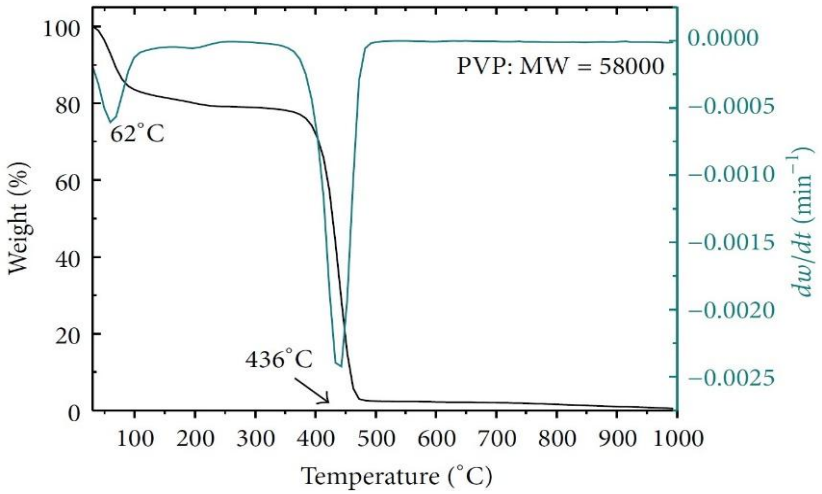

Figure 1: The original solution's thermogravimetric derivative (DTG) and thermogravimetric derivative (TG) curves at a heating rate of 10 °C/min.

3.2 Analysis of heat (thermal analysis-TGA/DTG)

The thermal analysis of the preparatory solution provides the optimal temperature for the calcination process and allows the optimization of the heat treatment program. Thermogravimetric analysis and its derivative form, TGA-DTG curves, were utilized for the first solution that was dried at 30 °C. The thermogram is well illustrated in Fig. 1. The TGA curve illustrates two stages of weight reduction. The first, small weight loss (roughly 22 %) occurred between 30 and 250 °C and was caused by acetate and retained moisture in the sample. The second, significant weight loss, which occurred between 400 and 470 °C, was caused by the breakdown of organic residues (such as PVP). The remaining material, which began at 471 °C, was almost pure PdO nanoparticles with a small amount of carbonaceous product that was excluded because of the overheated PVP component, according to FTIR, EDX, and XRD data. The significant, sharp peaks of the DTG curve, which peak at about 62 and 436 °C, respectively, further confirm the slight weight loss of trapped moisture and PVP combustion.

3.3 FTIR study of phase composition

Following calcination, the samples' FTIR spectra are shown in Fig. 2 in the wavenumber range of 280-4000 cm^{-1}.

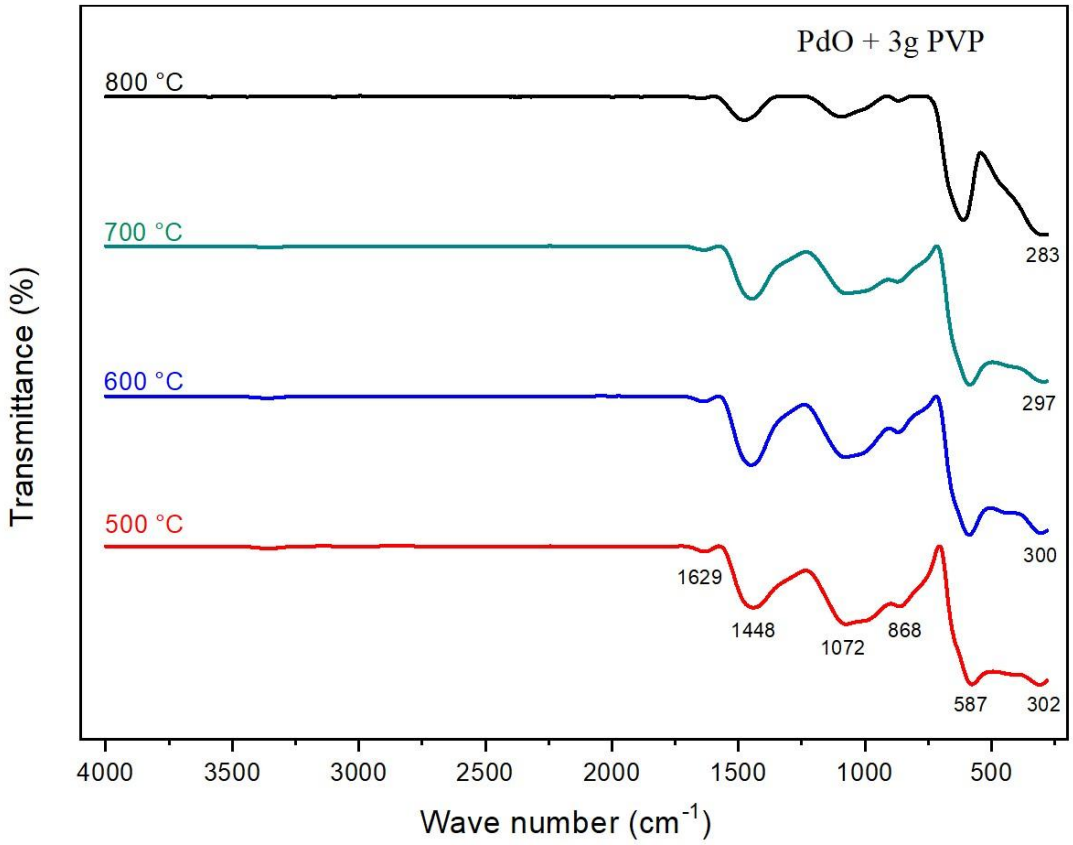

Figure 2: FTIR spectra of PdO nanoparticles at various calcination temperatures containing 3 g of PVP.

The absorption peaks at 1629 and 1448 cm^{-1} are the consequence of a vibration brought on by C–O and C–H bending in the methylene group, whereas the band at 1072 cm^{-1} is associated with a C–N stretching vibration. Conversely, the two peaks at 868 and 587 cm^{-1} are associated with vibrations brought on by the C–C ring and the C–N=O bending. The degradation of PVP utilized in sample preparation can be informally described as the relative loss of covalent bands of peaks between 4000 and 1000 cm^{-1} caused by calcining samples at 500 to 800 ^{o}C. Lastly, ionic bonds that conformed the development of crystalline PdO nanoparticles were the source of the remaining peaks at 302 cm^{-1} and below.

3.4 Analysis of elemental composition with EDX

Figure-3 displays the results of an EDX analysis of the elemental composition of PdO nanoparticles.

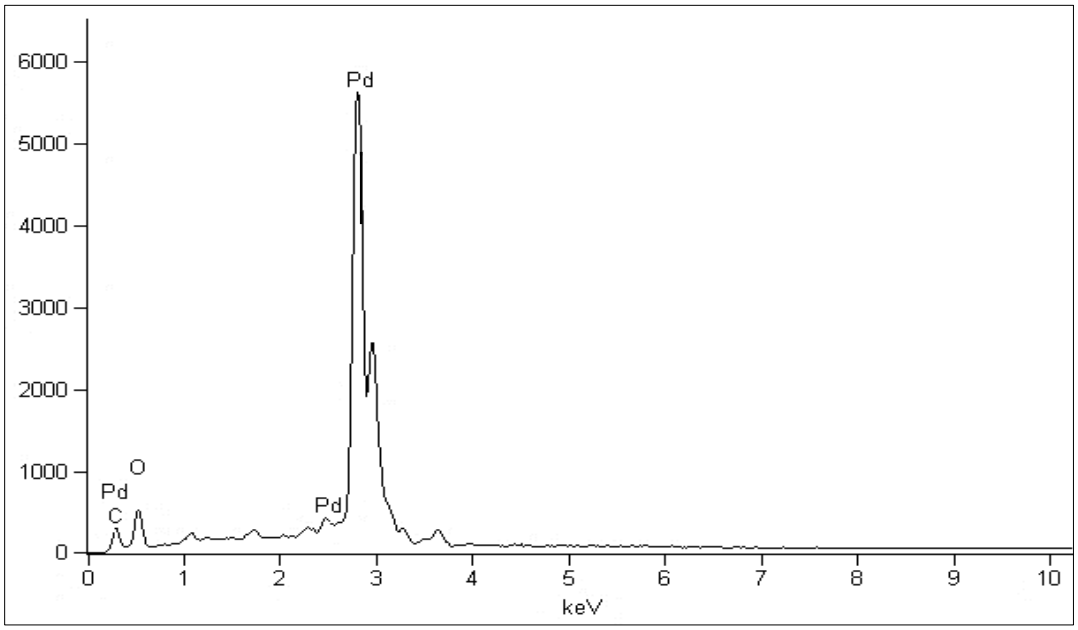

Figure 3: The EDX spectrum of PdO nanoparticles that were calcined at 600 °C.

Four elemental peaks can be seen in the host material of PdO nanoparticles: one for oxygen at 0.5 keV and three for palladium at 0.31, 2.53, and 2.97 keV. The weight ratio of Pd to O, based on EDX data, is approximately 70 to 25. The presence of certain low-intensity peaks in the spectrum is explained by the presence of carbon residue traces in the sample, which result from PVP's incomplete breakdown at 600 °C. As indicated in Table 1 below, the estimated weight ratio of carbon (C) residual in the samples at 0.30 is less than 5 %, allowing the reaction yield of palladium oxide nanoparticles to be.

Table 1: Estimated composition percentage of PdO nanoparticles and organic residuals at 600 ºC.

Element	Weight %	Weight Error %	Atom %	Atom Error %	Compound %	Norm. Compound %
C	4.06	+/- 0.11	12.96	+/- 0.35	4.06	4.06
O	25.70	+/- 0.61	61.69	+/- 1.46	25.70	25.70
Pd	70.24	+/- 0.67	25.35	+/- 0.24	70.24	70.24
Total	100		100		100	100

3.5 XRD structural analysis

By creating diffraction patterns from the crystalline powder samples at various temperatures in the 2θ range of 20°-70°, the crystal structure, crystallinity and crystallite size of produced PdO nanoparticles have been examined. Fig. 4 shows the XRD profile of the samples that were produced and thermally treated.

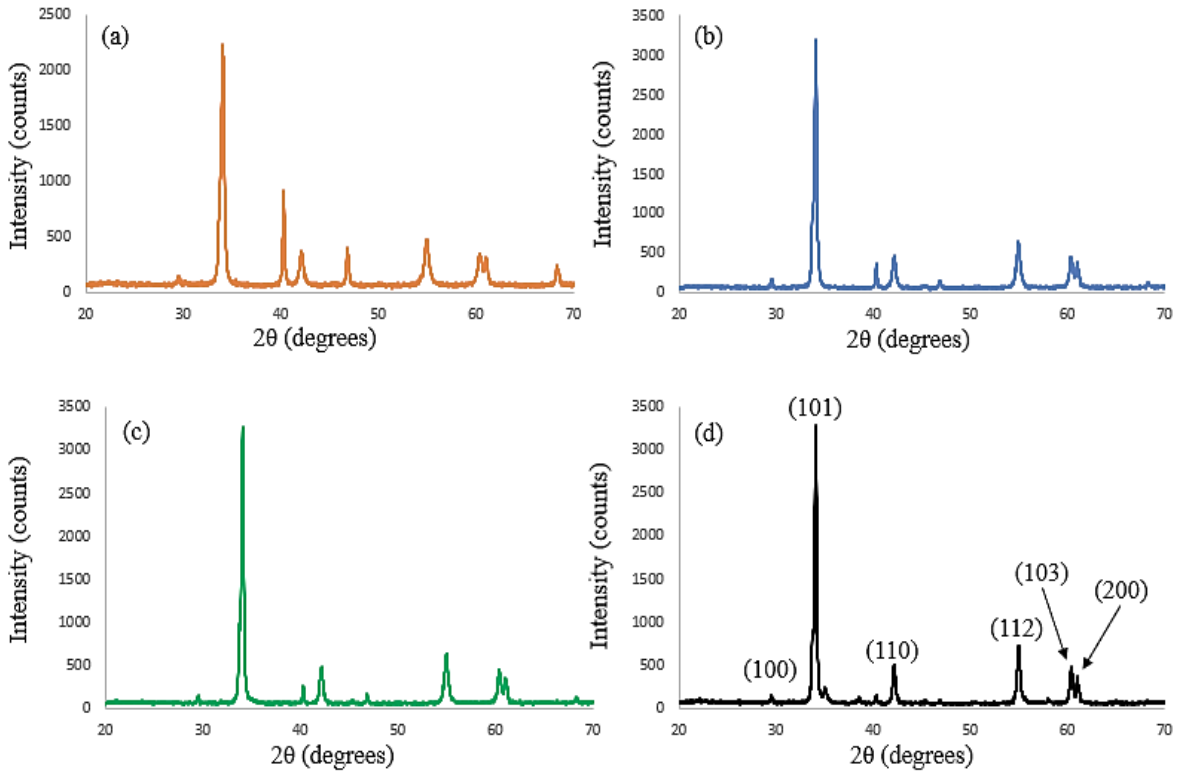

Figure 4: PdO nanoparticles' x-ray diffraction (XRD) pattern at various calcination temperatures. (a) 500 °C, (b) 600 °C, (c) 700 °C and (d) 800 °C.

Palladium oxide nanoparticles, as previously reported in [54], are assigned to the (100), (101), (110), (112), (103), and (200) planes (ICDD PDF 85-0713), which indicate the crystalline behavior of the sample as synthesized by applying varying calcination temperatures. The diffraction peaks become sharper and narrower as the calcination temperature rises, and their intensity noticeably increases. This indicates that the PdO nanocrystals' crystallinity has significantly improved, resulting from the increment of crystalline planes brought on by the enlargement of particle size [55]. The crystallite sizes were determined utilizing Scherrer's expression based on the full width at half maximum (FWHM) peak broadening of the (101) peak of the XRD patterns:

$$D = \frac{0.9\,\lambda}{\beta \cos\theta} \qquad (1)$$

When the x-ray wavelength (λ = 0.1542 nm), the angular line width of full width at half maximum (FWHM) intensity, the average crystallite size (D), and Bragg's angle (θ) are all taken into consideration. The computed crystallite sizes corresponding to various calcination temperatures are tabulated in Table-2.

Table 2: The crystal sizes and particle sizes that were measured at various calcination temperatures.

Sample °C	2θ	Crystallite size D_{XRD} (nm)	Particle size D_{TEM} (nm)
500	34.08	22	25
600	34.06	29	31
700	34.02	37	40
800	34.1	46	49

It is evident from the data in the above table that the crystallite size increases gradually as the calcination temperature grows, from 22 nm at 500 °C to 46 nm at 800 °C.

3.6 Morphology and size distribution analysis by TEM and FESEM

Figure-5 displays TEM images of semiconducting PdO nanoparticles at various calcination temperatures of 600, 700, and 800 °C. A consistent morphology with sufficient dispersion can be seen from the figure. The particle size distribution, which has a growth process and is dependent on the calcination temperature, is between about 25 and 68 nm. When the capping PVP polymer gradually broke down during calcination, which began at around 471 °C, a nucleation process began in which Pd^{-2} reacted with two O^{+2} from the air to form PdO^0 molecules. These molecules were then uniformly distributed and immediately underwent agglomeration to form PdO^0 2 or PdO^0 m ($m > 2$) nanoparticles. At higher calcination temperatures, massive PdO^0 m nanoparticles can further aggregate with additional PdO^0 n nanoparticles to generate even larger PdO^0 m+n nanoparticles. The loss of carbon traces (see Fig. 1) from the particle surface, which caused nearby particles to clump together and eventually form larger particles, is thought to be the cause of the particle size increase with calcination temperature. The average particle sizes obtained from TEM images are in a good agreement with the XRD profile results presented in Table-2 [68].

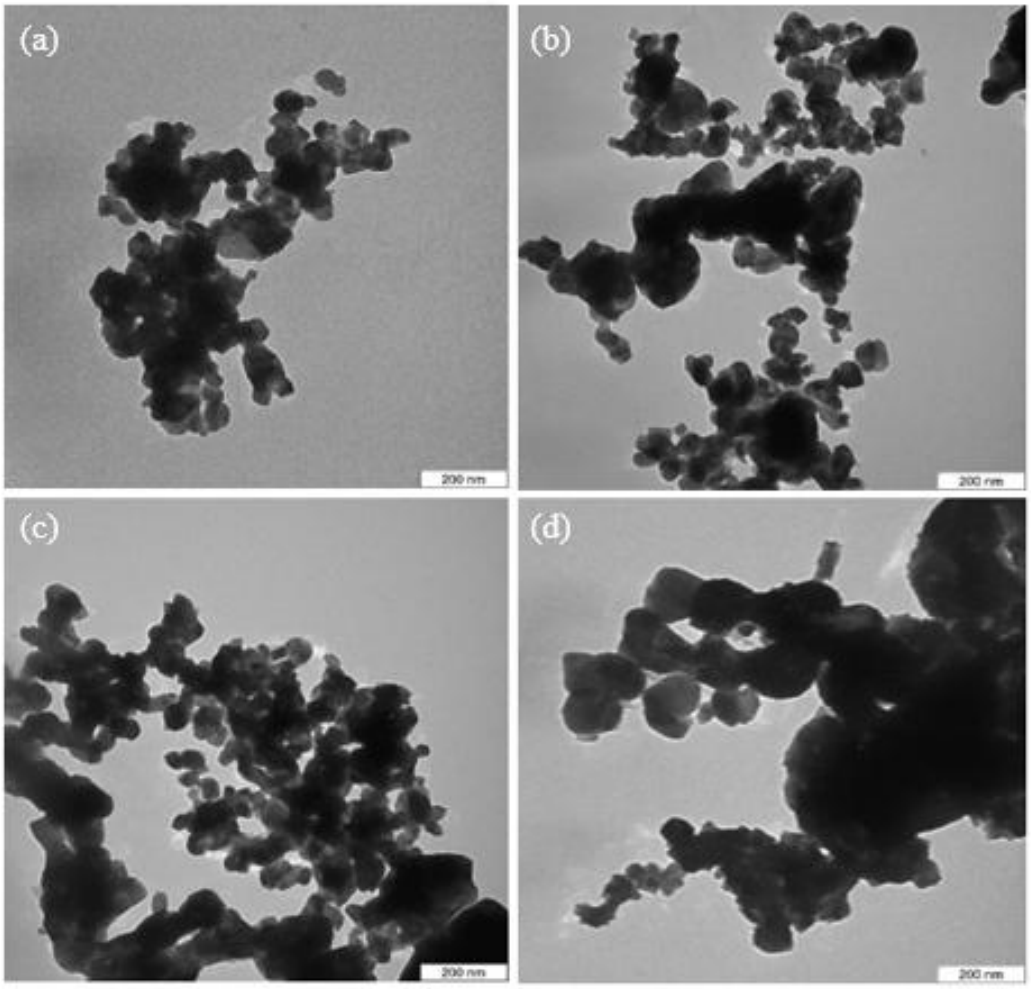

Figure 5: The PdO nanoparticles' TEM images at (a) 500, (b) 600, (c) 700 and (d) 800 °C at various calcination temperatures.

As seen in Fig. 6, the surface morphology of palladium oxide nanoparticles, which were produced by heat treatment; was also examined using the field emission scanning electron microscopy (FESEM) technique. A 5 kV operating voltage was used to take the pictures. The pictures illustrate how PdO forms at four distinct calcination temperatures when a capping modulator, or PVP, is present. It is clear to see that, the structures were inconsistently distributed and aggregated to form crystal structures (quasi-spherical shape), which then attached to each other to form larger connected crystal shapes as shown in Fig. 6 (b, c and d) [69-70]. With increasing temperature more crystal structures starts to shape up and gradually grow from the nanoscale size to bulk scale, where all the properties will start to change back. The morphology is rather porous and composed of assembly of globular structures decorated with a number of smaller NPs with typical sizes of about 20 – 50 nm [71]. It is notable that Palladium crystalline phase can be seen with higher calcination temperatures, i.e., 800 ºC. Therefore, fabrication of Palladium oxide nanoparticles by thermal treatment can be valid by using capping agent and calcination temperatures below 800 ºC.

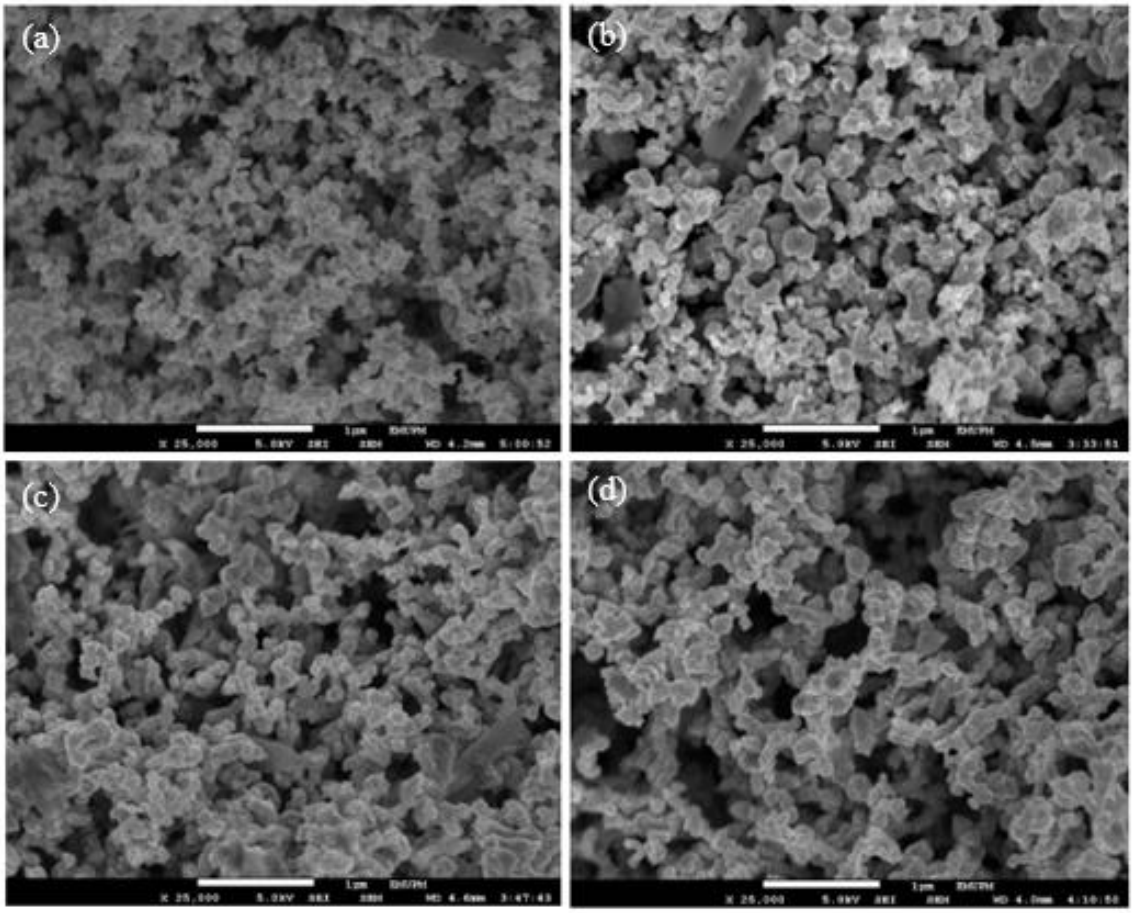

Figure 6: X = 25,000 magnification FESEM pictures of the topography of PdO nanoparticles at (a) 500, (b) 600, (c) 700, and (d) 800 ºC calcination temperatures.

3.7 Optical properties

Using the Kubelka-Munk equation, the optical band gap energies for the calcined materials at various temperatures were obtained from reflectance spectra as shown below:

$$(F(R\infty).hv)^2 = A(hv - Eg) \qquad (2)$$

The re-emission parameter or Kubelka-Munk function is indicated as $F(R_\infty)$, $h\nu$ is the incident photon energy, R_∞ is the diffuse reflectance, that is obtained from $R_\infty = R_{sample} / R_{standard}$ and A is a constant depending on the transition probability and the diffuse reflectance R_∞ [72]. For the calcined materials at various temperatures, Fig. 7 showed the values of $(F(R\infty)\cdot h\nu)^2$

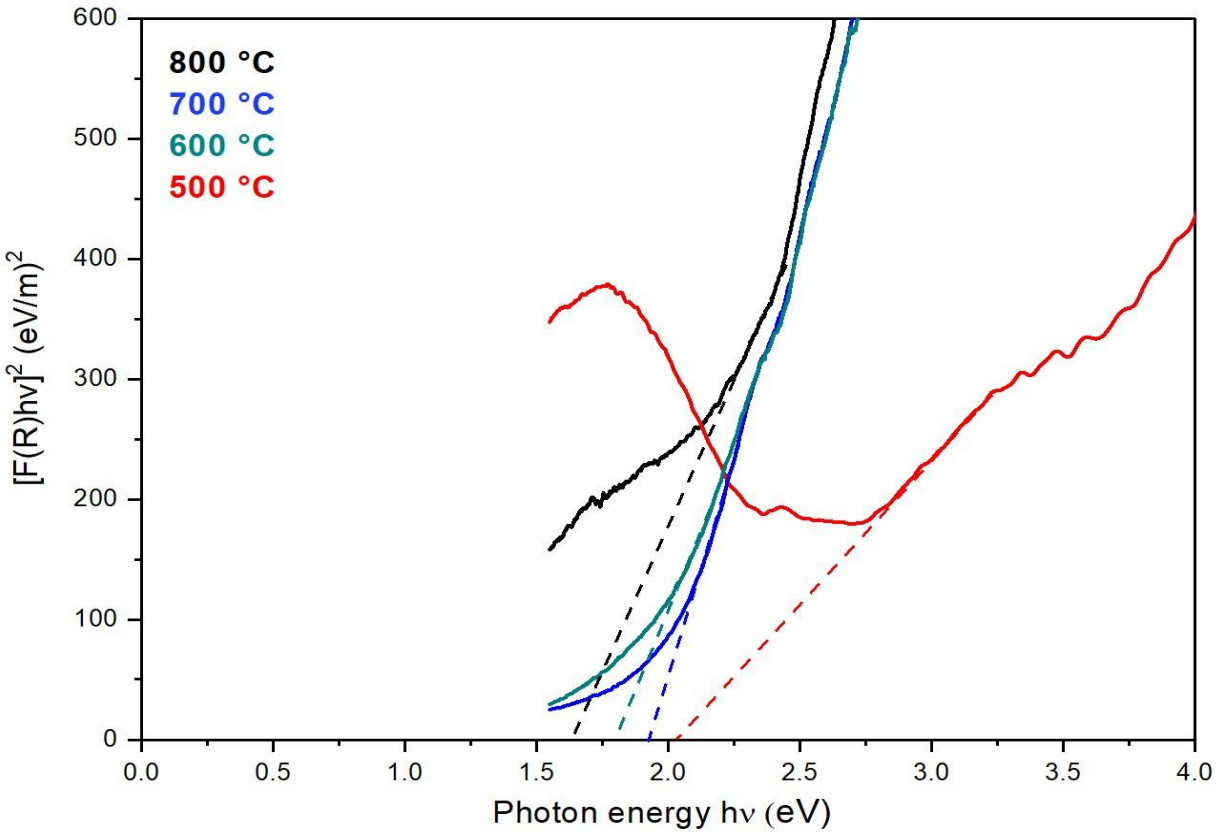

Figure 7: The graph of the calcined samples' square Kubelka-Munk function vs photon energy at various temperatures.

The optical band gap values of the PdO nanoparticles at different temperatures of calcination have been estimated by drawing straight lines to suit the data curves and then prolonging them to cut off the x-axis. According to Table-2, it was discovered that the optical direct band gap reduced as the calcination temperature increased, going from 2.09 eV at 500 °C to 1.63 eV at 800 °C. The decrement of the energy band gap with increasing the calcination temperatures is credited to the growth of the particle and the crystallinity improvement according to the XRD analysis [73-74]. It is supposed that, as the particle size increases, the number of atoms that form a particle also increases, consequently rendering the valence and conduction electrons more attractive to the ions core of the particles and hence decreasing the band gap of the particles [62, 75]. Perhaps the contribution of the phonons has a role in trapping electrons and consequently influences the band gap energy level during optical properties measurement [63, 76].

4 Conclusion

By directly calcining an aqueous solution comprising palladium (II) nitrate dehydrates as a metal precursor and polyvinylpyrrolidone as a capping mediator, palladium oxide nanoparticles have been effectively produced. The organic compounds were effectively removed during the calcination process by the current thermal treatment method, which does not include drying, leaving behind crystalline PdO nanoparticle residue. Furthermore, it was discovered that the calcination temperature has a crucial role in regulating the average particle size, which ranges from 25 to 49 nm when the temperature is raised from 500 to 800 °C, respectively. This modified thermal treatment route to synthesize PdO nanoparticles is a very simple, economical, and environmentally friendly method that could be used for large-scale industrial fabrication of metallic nano oxides. As the size of the particles increased, the band gap energy of PdO nanoparticles decreased from 2.09 eV at 500 °C to 1.63 eV at 800 °C.

ACKNOWLEDGMENTS

The staff of Universiti Putra Malaysia's Faculty of Science and Institute of Bioscience (IBS) provided technical assistance, which the authors would like to thank. The authors also acknowledge Middle Technical University and Koya University for making this work possible.

FUNDING

Our gratitude to The Research Management Center (RMC) of Universiti Putra Malaysia provided financial assistance for this endeavor.

AUTHOR DECLIRATIONS

Conflict of interest

The authors have no conflicts to disclose.

Author contributions

Ayser S. Keiteb: Writing original draft, review, editing, resources, methodology and investigation.
Mohammed M. Sabri: Writing, review, editing and supervision.

DATA AVAILABILITY

The data that support the findings of this study are available from the corresponding author upon reasonable request.

References

[1] Rabiee, N., Bagherzadeh, M., Kiani, M. and Ghadiri, A.M., 2020. Rosmarinus officinalis directed palladium nanoparticle synthesis: investigation of potential anti-bacterial, anti-fungal and Mizoroki-Heck catalytic activities. *Advanced Powder Technology*, *31*(4), pp.1402-1411.

[2] Burda, C., Chen, X., Narayanan, R. and El-Sayed, M.A., 2005. Chemistry and properties of nanocrystals of different shapes. *Chemical reviews*, *105*(4), pp.1025-1102.

[3] Joudeh, N., Saragliadis, A., Koster, G., Mikheenko, P. and Linke, D., 2022. Synthesis methods and applications of palladium nanoparticles: A review. *Frontiers in Nanotechnology*, *4*, p.1062608.

[4] Hirvonen, A., Nowak, R., Yamamoto, Y., Sekino, T. and Niihara, K., 2006. Fabrication, structure, mechanical and thermal properties of zirconia-based ceramic nanocomposites. *Journal of the European Ceramic Society*, *26*(8), pp.1497-1505.

[5] Abou El-Nour, K.M., Eftaiha, A.A., Al-Warthan, A. and Ammar, R.A., 2010. Synthesis and applications of silver nanoparticles. *Arabian journal of chemistry*, *3*(3), pp.135-140.

[6] Saldan, I., Semenyuk, Y., Marchuk, I. and Reshetnyak, O., 2015. Chemical synthesis and application of palladium nanoparticles. *Journal of Materials Science*, *50*, pp.2337-2354.

[7] Chen, Y.H., Hung, H.H. and Huang, M.H., 2009. Seed-mediated synthesis of palladium nanorods and branched nanocrystals and their use as recyclable Suzuki coupling reaction catalysts. *Journal of the American Chemical Society*, *131*(25), pp.9114-9121.

[8] Phan, T.T.V., Hoang, G., Nguyen, T.P., Kim, H.H., Mondal, S., Manivasagan, P., Moorthy, M.S., Lee, K.D. and Junghwan, O., 2019. Chitosan as a stabilizer and size-control agent for synthesis of porous flower-shaped palladium nanoparticles and their applications on photo-based therapies. *Carbohydrate polymers*, *205*, pp.340-352.

[9] Anila, P.A., Keerthiga, B., Ramesh, M. and Muralisankar, T., 2021. Synthesis and characterization of palladium nanoparticles by chemical and green methods: A comparative study on hepatic toxicity using zebrafish as an animal model. *Comparative Biochemistry and Physiology Part C: Toxicology & Pharmacology*, *244*, p.108979.

[10] Wilson, O.M., Knecht, M.R., Garcia-Martinez, J.C. and Crooks, R.M., 2006. Effect of Pd nanoparticle size on the catalytic hydrogenation of allyl alcohol. *Journal of the American Chemical Society*, *128*(14), pp.4510-4511.

[11] Karimi, B. and Enders, D., 2006. New N-heterocyclic carbene palladium complex/ionic liquid matrix immobilized on silica: Application as recoverable catalyst for the Heck reaction. *Organic Letters*, *8*(6), pp.1237-1240.

[12] Petla, R.K., Vivekanandhan, S., Misra, M., Mohanty, A.K. and Satyanarayana, N., 2011. Soybean (Glycine max) leaf extract based green synthesis of palladium nanoparticles.

[13] Chu, J., Ma, H., Zhang, L. and Wang, Z., 2021. Biomass-derived paper-based nanolignin/palladium nanoparticle composite film for catalytic reduction of hexavalent chromium. *Industrial Crops and Products*, *165*, p.113439.

[14] Aditya, T., Pal, A. and Pal, T., 2015. Nitroarene reduction: a trusted model reaction to test nanoparticle catalysts. *Chemical Communications*, *51*(46), pp.9410-9431.

[15] Narayanan, R. and El-Sayed, M.A., 2005. Carbon-supported spherical palladium nanoparticles as potential recyclable catalysts for the Suzuki reaction. *Journal of Catalysis*, *234*(2), pp.348-355.

[16] Cheong, S., Watt, J.D. and Tilley, R.D., 2010. Shape control of platinum and palladium nanoparticles for catalysis. *Nanoscale*, *2*(10), pp.2045-2053.

[17] Bianchini, C. and Shen, P.K., 2009. Palladium-based electrocatalysts for alcohol oxidation in half cells and in direct alcohol fuel cells. *Chemical reviews*, *109*(9), pp.4183-4206.

[18] Yamauchi, M., Ikeda, R., Kitagawa, H. and Takata, M., 2008. Nanosize effects on hydrogen storage in palladium. *The Journal of Physical Chemistry C*, *112*(9), pp.3294-3299.

[19] Shaik, M.R., Ali, Z.J.Q., Khan, M., Kuniyil, M., Assal, M.E., Alkhathlan, H.Z., Al-Warthan, A., Siddiqui, M.R.H., Khan, M. and Adil, S.F., 2017. Green synthesis and characterization of palladium nanoparticles using Origanum vulgare L. extract and their catalytic activity. *Molecules*, *22*(1), p.165.

[20] Mubeen, S., Zhang, T., Yoo, B., Deshusses, M.A. and Myung, N.V., 2007. Palladium nanoparticles decorated single-walled carbon nanotube hydrogen sensor. *The Journal of Physical Chemistry C*, *111*(17), pp.6321-6327.

[21] Tobiška, P., Hugon, O., Trouillet, A. and Gagnaire, H., 2001. An integrated optic hydrogen sensor based on SPR on palladium. *Sensors and Actuators B: Chemical*, *74*(1-3), pp.168-172.

[22] Rahimi-Mohseni, M., Raoof, J.B., Ojani, R., Aghajanzadeh, T.A. and Hashkavayi, A.B., 2018. Development of a new paper-based nano-biosensor using the co-catalytic effect of tyrosinase from banana peel tissue (Musa Cavendish) and functionalized silica nanoparticles for voltammetric determination of L-tyrosine. *International journal of biological macromolecules*, *113*, pp.648-654.

[23] Popa, C., Zhu, T., Tranca, I., Kaghazchi, P., Jacob, T. and Hensen, E.J., 2015. Structure of palladium nanoparticles under oxidative conditions. *Physical Chemistry Chemical Physics*, *17*(3), pp.2268-2273.

[24] Kibis, L.S., Stadnichenko, A.I., Koscheev, S.V., Zaikovskii, V.I. and Boronin, A.I., 2012. Highly oxidized palladium nanoparticles comprising Pd4+ species: spectroscopic and structural aspects, thermal stability, and reactivity. *The Journal of Physical Chemistry C*, *116*(36), pp.19342-19348.

[25] Heard, C.J., Vajda, S. and Johnston, R.L., 2014. Support and oxidation effects on subnanometer palladium nanoparticles. *The Journal of Physical Chemistry C*, *118*(7), pp.3581-3589.

[26] Xu, H. and Suslick, K.S., 2010. Sonochemical synthesis of highly fluorescent Ag nanoclusters. *ACS nano*, *4*(6), pp.3209-3214.

[27] Cui, Y., Zhu Chen, J., Peng, B., Kovarik, L., Devaraj, A., Li, Z., Ma, T., Wang, Y., Szanyi, J., Miller, J.T. and Wang, Y., 2021. Onset of high methane combustion rates over supported palladium catalysts: from isolated Pd cations to PdO nanoparticles. *JACS Au*, *1*(4), pp.396-408.

[28] Gong, M., Li, X., Hu, L., Xu, H., Yang, C., Luo, Y., Li, S., Yin, C., Gan, M. and Zhou, L., 2024. Preparation and characterization of palladium nanoparticle-embedded carbon nanofiber membranes via electrospinning and carbonization strategy. *RSC advances*, *14*(30), pp.21623-21634.

[29] Zorn, K., Giorgio, S., Halwax, E., Henry, C.R., Gronbeck, H. and Rupprechter, G., 2011. CO oxidation on technological Pd− Al2O3 catalysts: oxidation state and activity. *The Journal of Physical Chemistry C*, *115*(4), pp.1103-1111.

[30] Zhu, G., Han, J., Zemlyanov, D.Y. and Ribeiro, F.H., 2005. Temperature dependence of the kinetics for the complete oxidation of methane on palladium and palladium oxide. *The Journal of Physical Chemistry B*, *109*(6), pp.2331-2337.

[31] Jana, N.R., Wang, Z.L. and Pal, T., 2000. Redox catalytic properties of palladium nanoparticles: surfactant and electron donor− acceptor effects. *Langmuir*, *16*(6), pp.2457-2463.

[32] Boronin, A.I., Slavinskaya, E.M., Danilova, I.G., Gulyaev, R.V., Amosov, Y.I., Kuznetsov, P.A., Polukhina, I.A., Koscheev, S.V., Zaikovskii, V.I. and Noskov, A.S., 2009. Investigation of palladium interaction with cerium oxide and its state in catalysts for low-temperature CO oxidation. *Catalysis today*, *144*(3-4), pp.201-211.

[33] Oh, S.H. and Hoflund, G.B., 2007. Low-temperature catalytic carbon monoxide oxidation over hydrous and anhydrous palladium oxide powders. *Journal of Catalysis*, *245*(1), pp.35-44.

[34] Lichtenberger, J., Lee, D. and Iglesia, E., 2007. Catalytic oxidation of methanol on Pd metal and oxide clusters at near-ambient temperatures. *Physical Chemistry Chemical Physics*, *9*(35), pp.4902-4906.

[35] Liu, L., Yoo, S.H., Lee, S.A. and Park, S., 2011. Wet-chemical synthesis of palladium nanosprings. *Nano letters*, *11*(9), pp.3979-3982.

[36] Remillard, J.T., Weber, W.H., McBride, J.R. and Soltis, R.E., 1992. Optical studies of PdO thin films. *Journal of applied physics*, *71*(9), pp.4515-4522.

[37] Park, D.W. and Ray, J.C., 2006. Chemical synthesis of stabilized nanocrystalline zirconia powders. *Journal of Industrial and Engineering Chemistry*, *12*(1), pp.142-148.

[38] Gole, J.L., Prokes, S.M., Stout, J.D., Glembocki, O.J. and Yang, R., 2006. Unique properties of selectively formed zirconia nanostructures. *Advanced Materials*, *18*(5), pp.664-667.

[39] Badica, P. and Lőrinczi, A., 2024. A Review on Preparation of Palladium Oxide Films. *Coatings*, *14*(10), p.1260.

[40] Usoltsev, O., Stoian, D., Skorynina, A., Kozyr, E., Njoroge, P.N., Pellegrini, R., Groppo, E., van Bokhoven, J.A. and Bugaev, A., 2024. Restructuring of palladium nanoparticles during oxidation by molecular oxygen. *Small*, *20*(42), p.2401184.

[41] Oh, D.G., Aleksandrov, H.A., Kim, H., Koleva, I.Z., Khivantsev, K., Vayssilov, G.N. and Kwak, J.H., 2023. Understanding of Active Sites and Interconversion of Pd and PdO during CH4 Oxidation. *Molec*

[42] Alaqarbeh, M., Adil, S.F., Ghrear, T., Khan, M., Bouachrine, M. and Al-Warthan, A., 2023. Recent progress in the application of palladium nanoparticles: a review. *Catalysts*, *13*(10), p.1343.

[43] Kadu, B.S., 2021. Suzuki–Miyaura cross coupling reaction: recent advancements in catalysis and organic synthesis. *Catalysis Science & Technology*, *11*(4), pp.1186-1221.

[44] Park, S., Vohs, J.M. and Gorte, R.J., 2000. Direct oxidation of hydrocarbons in a solid-oxide fuel cell. *Nature*, *404*(6775), pp.265-267.

[45] Piermatti, O., 2021. Green synthesis of Pd nanoparticles for sustainable and environmentally benign processes. *Catalysts*, *11*(11), p.1258.

[46] Chen, A. and Ostrom, C., 2015. Palladium-based nanomaterials: synthesis and electrochemical applications. *Chemical Reviews*, *115*(21), pp.11999-12044.

[47] Ismail, E., Khenfouch, M., Dhlamini, M., Dube, S. and Maaza, M., 2017. Green palladium and palladium oxide nanoparticles synthesized via Aspalathus linearis natural extract. *Journal of Alloys and Compounds*, *695*, pp.3632-3638.

[48] Drummer, Sean, Tafirenyika Drummer, S., Madzimbamuto, T. and Chowdhury, M., 2021. Green synthesis of transition-metal nanoparticles and their oxides: a review. *Materials*, *14*(11), p.2700.

[49] Siddiqi, K.S. and Husen, A., 2016. Green synthesis, characterization and uses of palladium/platinum nanoparticles. *Nanoscale research letters*, *11*, pp.1-13.

[50] Savadogo, O., Lee, K., Oishi, K., Mitsushima, S., Kamiya, N. and Ota, K.I., 2004. New palladium alloys catalyst for the oxygen reduction reaction in an acid medium. *Electrochemistry communications*, *6*(2), pp.105-109.

[51] Farella, I., Valentini, A., Cioffi, N. and Torsi, L., 2005. Dual ion-beam sputtering deposition of palladium-fluoropolymer nano-composites. *Applied Physics A*, *80*, pp.791-795.

[52] Ebenezer, J., Lal, A., Velayudham, P., Borenstein, A. and Schechter, A., 2024. Laser-Induced Pd-PdO/rGO Catalysts for Enhanced Electrocatalytic Conversion of Nitrate into Ammonia. *ACS Applied Materials & Interfaces*, *16*(28), pp.36433-36443.

[53] Nánai, L. and Balint, A.M., 2012, August. Laser Induced Chemical Liquid Phase Deposition (LCLD). In *AIP Conference Proceedings* (Vol. 1472, No. 1, pp. 148-154). American Institute of Physics.

[54] Kumari, T., Gopal, R., Goyal, A. and Joshi, J., 2019. Sol–gel synthesis of Pd@ PdO core–shell nanoparticles and effect of precursor chemistry on their structural and optical properties. *Journal of Inorganic and Organometallic Polymers and Materials*, *29*, pp.316-325.

[55] Muniz-Miranda, M., Zoppi, A., Muniz-Miranda, F. and Calisi, N., 2020. Palladium oxide nanoparticles: Preparation, characterization and catalytic activity evaluation. *Coatings*, *10*(3), p.207.

[56] Thoda, O., Xanthopoulou, G., Vekinis, G. and Chroneos, A., 2018. Review of recent studies on solution combustion synthesis of nanostructured catalysts. *Advanced Engineering Materials*, *20*(8), p.1800047.

[57] Li, Z., Song, J., Lee, D.C., Abdelhafiz, A., Xiao, Z., Hou, Z., Liao, S., DeGlee, B., Liu, M., Zeng, J. and Alamgir, F.M., 2020. Mono-disperse PdO nanoparticles prepared via microwave-assisted thermo-hydrolyzation with unexpectedly high activity for formic acid oxidation. *Electrochimica Acta*, *329*, p.135166.

[58] Sekiguchi, Y., Hayashi, Y. and Takizawa, H., 2011. Synthesis of palladium nanoparticles and palladium/spherical carbon composite particles in the solid–liquid system of palladium oxide–alcohol by microwave irradiation. *Materials transactions*, *52*(5), pp.1048-1052.

[59] Wu, M.C., Hsiao, K.C., Chang, Y.H. and Chan, S.H., 2018. Photocatalytic hydrogen evolution of palladium nanoparticles decorated black TiO2 calcined in argon atmosphere. *Applied Surface Science*, *430*, pp.407-414.

[60] Wang, K., Huang, T., Liu, H., Zhao, Y., Liu, H. and Sun, C., 2008. Size control synthesis of palladium oxide nanoparticles by microwave irradiation. *Colloids and Surfaces A: Physicochemical and Engineering Aspects*, *325*(1-2), pp.21-25.

[61] Bagchi, V. and Bandyopadhyay, D., 2009. In situ generation of palladium oxide nano-crystals. *Journal of Organometallic Chemistry*, *694*(9-10), pp.1259-1262.

[62] Keiteb, A.S., Saion, E., Zakaria, A. and Soltani, N., 2016. Structural and optical properties of zirconia nanoparticles by thermal treatment synthesis. *Journal of nanomaterials*, *2016*(1), p.1913609.

[63] Keiteb, A.S., Saion, E., Zakaria, A., Soltani, N. and Abdullahi, N., 2016. A modified thermal treatment method for the up-scalable synthesis of size-controlled nanocrystalline titania. *Applied Sciences*, *6*(10), p.295.

[64] Wiley, B., Sun, Y., Mayers, B. and Xia, Y., 2005. Shape-controlled synthesis of metal nanostructures: the case of silver. *Chemistry–A European Journal*, *11*(2), pp.454-463.

[65] Zheng, Y., Cheng, Y., Wang, Y., Bao, F., Zhou, L., Wei, X., Zhang, Y. and Zheng, Q., 2006. Quasicubic α-Fe2O3 nanoparticles with excellent catalytic performance. *The Journal of Physical Chemistry B*, *110*(7), pp.3093-3097.

[66] Soltani, N., Saion, E., Hussein, M.Z., Erfani, M., Rezaee, K. and Bahmanrokh, G., 2012. Phase controlled monodispersed CdS nanocrystals synthesized in polymer solution using microwave irradiation. *Journal of Inorganic and Organometallic Polymers and Materials*, *22*, pp.830-836.

[67] Naseri, M.G., Saion, E.B., Ahangar, H.A., Hashim, M. and Shaari, A.H., 2011. Simple preparation and characterization of nickel ferrite nanocrystals by a thermal treatment method. *Powder Technology*, *212*(1), pp.80-88.

[68] José-Yacamán, M., Marın-Almazo, M. and Ascencio, J.A., 2001. High resolution TEM studies on palladium nanoparticles. *Journal of Molecular Catalysis A: Chemical*, *173*(1-2), pp.61-74.

[69] Veisi, H., Karmakar, B., Tamoradi, T., Tayebee, R., Sajjadifar, S., Lotfi, S., Maleki, B. and Hemmati, S., 2021. Bio-inspired synthesis of palladium nanoparticles fabricated magnetic Fe3O4 nanocomposite over Fritillaria imperialis flower extract as an efficient recyclable catalyst for the reduction of nitroarenes. *Scientific Reports*, *11*(1), p.4515.

[70] Sandaruwan, C., Herath, H. M. P. C. K., Karunarathne, T. S. E. F., Ratnayake, S. P., Amaratunga, G. A. J., & Dissanayake, D. P. (2018). Polyaniline/palladium nanohybrids for moisture and hydrogen detection. *Chemistry Central Journal*, *12*(1), 93.

[71] Thuan, N.D., Cuong, H.M., Nam, N.H., Huong, N.T.L. and Hong, H.S., 2024. Morphological analysis of Pd/C nanoparticles using SEM imaging and advanced deep learning. *RSC advances*, *14*(47), pp.35172-35183.

[72] Makuła, P., Pacia, M. and Macyk, W., 2018. How to correctly determine the band gap energy of modified semiconductor photocatalysts based on UV–Vis spectra. *The journal of physical chemistry letters*, *9*(23), pp.6814-6817.

[73] Matussin, S.N., Khan, F., Harunsani, M.H., Kim, Y.M. and Khan, M.M., 2023. Effect of Pd-doping concentrations on the photocatalytic, photoelectrochemical, and photoantibacterial properties of CeO2. *Catalysts*, *13*(1), p.96.

[74] Vikal, S., Gautam, Y.K., Kumar, A., Kumar, A., Singh, J., Pratap, D., Singh, B.P. and Singh, N., 2023. Bioinspired palladium-doped manganese oxide nanocorns: A remarkable antimicrobial agent targeting phyto/animal pathogens. *Scientific Reports*, *13*(1), p.14039.

[75] Mayedwa, N., Mongwaketsi, N., Khamlich, S., Kaviyarasu, K., Matinise, N. and Maaza, M., 2018. Green synthesis of nickel oxide, palladium and palladium oxide synthesized via Aspalathus

linearis natural extracts: physical properties & mechanism of formation. *Applied Surface Science*, *446*, pp.266-272.

[76] Omotunde, O.I., Okoronkwo, A.E., Aiyesanmi, A.F. and Gurgur, E., 2018. Photocatalytic behavior of mixed oxide NiO/PdO nanoparticles toward degradation of methyl red in water. *Journal of Photochemistry and Photobiology A: Chemistry*, *365*, pp.145-150.